Journal of Oceanology and Limnology
Vol. 41 No. 3, P. 831-851, 2023
https://doi.org/10.1007/s00343-022-1237-8

Interannual variability of eddy kinetic energy in the South China Sea related to two types of winter circulation events*

Wenlian LI[1, 2], Qinyan LIU[2, 3, **], Wendong FANG[2, 3], Tingting ZU[2, 3], Haiying CHEN[4, 5, 6]

[1] *University of Chinese Academy of Sciences*, *Beijing 100049*, *China*
[2] *South China Sea Institute of Oceanology*, *Chinese Academy of Sciences*, *Guangzhou 528200*, *China*
[3] *Southern Marine Science and Engineering Guangdong Laboratory* (*Guangzhou*), *Guangzhou 528200*, *China*
[4] *CAS Key Laboratory of Ocean Circulation and Waves*, *Institute of Oceanology*, *Chinese Academy of Sciences*, *Qingdao 266071*, *China*
[5] *Pilot National Laboratory for Marine Science and Technology* (*Qingdao*), *Qingdao 266237*, *China*
[6] *Center for Ocean Mega-Science*, *Chinese Academy of Sciences*, *Qingdao 266071*, *China*

Received Jul. 20, 2021; accepted in principle Oct. 11, 2021; accepted for publication Feb. 14, 2022

Abstract Interannual variations of the eddy kinetic energy (EKE) related to two types of winter circulation events ("O" and "U") were investigated based on the outputs of the Ocean General Circulation Model (OGCM) for the Earth Simulator (OFES) and the corresponding energetic analyses. Results show that the EKE is strong and extends eastward to offshore the Vietnam coast about 2°, associated with the weaker South China Sea western boundary current (SCSwbc) in "O" type years, while the EKE is weak and high value that can be attained is narrowed along the coast, associated with the stronger SCSwbc in "U" type years. The energy budget shows that the wind stress and barotropic/baroclinic instability are important factors to regulate the EKE in "U" and "O" years. For "U" years, under a strong winter monsoon forcing, the SCSwbc strengthen, the directly wind work and barotropic conversion from the mean kinetic energy (MKE) to EKE are weak, thus the EKE decrease corresponding to the baroclinic conversion from the kinetic energy to potential energy. However, the situation is reversed in "O" years. Under the influence of El Niño events, wind stress forces can weaken SCSwbc and enhance EKE in pattern "O", whereas La Niña events have relatively weaker influences. The barotropic conversion rate in "O" type is nearly eight times of the "U" type. The pressure work and advection term are the main sources to greatly suppress EKE in the SCSwbc region.

Keyword: two-type winter circulation; South China Sea western boundary current; energy budget

1 INTRODUCTION

Mesoscale eddies are a natural phenomenon occurring in oceans all around the world (Chelton et al., 2011). The South China Sea (SCS) is the largest semi-enclosed marginal sea in Southeast Asia (Fig.1). Because of the seasonally reversing monsoon, wind-driven circulation is the main component of the general circulation in the SCS (Dale, 1956; Wyrtki, 1961). Seasonal circulation is predominant in the SCS (Hu et al., 2000; Liu et al., 2001), and it appears as a multi-eddy structure (Shaw et al., 1999; Su et al., 1999, 2002; Fang et al., 2002). The origin of seasonal circulation is mainly attributed to wind, the nonlinear effect of currents, eddy shedding, penetration of nonlinear Rossby eddies into the SCS, and topography (Hwang and Chen, 2000; Metzger

* Supported by the Science and Technology Basic Resources Investigation Program of China (No. 2017FY201402), the Southern Marine Science and Engineering Guangdong Laboratory (Guangzhou) (No. GML 2019ZD0304), the National Key Research and Development Program of China (No. 2017YFC1404000), the National Natural Science Foundation of China (Nos. 41876017, 42176027, 41628601, 41706027, 41776014), the Guangzhou Science and Technology Plan Project (No. 202102080364), the Guangdong Basic and Applied Basic Research Foundation (No. 2022A1515011863), and the State Key Laboratory of Tropical Oceanography, South China Sea Institute of Oceanology Chinese Academy of Sciences (Nos. LTOZZ2101, LTOZZ2102)
** Corresponding author: qyliu66@scsio.ac.cn

and Hurlburt, 2001; Wang et al., 2003, 2008a, b; Xie et al., 2003; Yuan et al., 2007; Gan and Qu, 2008; Hu et al., 2012; Chen et al., 2015). Ocean eddies, as analogous weather systems in the atmosphere, are an important mechanism for the transport of heat, momentum, and matter (Holloway, 1986). Thus, they are an important component in ocean dynamics, marine ecosystems, and air-sea interaction (McGillicuddy et al., 2007; Frenger et al., 2013; Dong et al., 2014; Ma et al., 2016).

In the SCS, eddies are active along the continental slope from southern Vietnam to the southwest of Taiwan, China (Ho et al., 2000; Wang et al., 2000, 2003; Lin et al., 2007; Zhuang et al., 2010). Wang et al. (2003) showed that eddies are mainly grouped into four geographic zones according to eddy generation mechanisms. Despite the discrepancy in statistical characteristic of SCS eddies in Xiu et al. (2010) and Wang et al. (2003), perhaps caused by the different criteria and dataset used in identifying eddies, they both pointed out the high-occurrence of eddies locates at offshore of Vietnam. Eddies in this area embedded in the western boundary current (WBC) have strong intra-seasonal, seasonal and interannual variability (Xiu et al., 2010; Zhuang et al., 2010; Chen et al., 2011). Strong intra-seasonal sea surface height variability is found in the southeast of Vietnam, exhibiting clear seasonal variations (Zhuang et al., 2010). The eddy propagation from the western basin to the east of Vietnam is random (Chen et al., 2011). Anticyclonic eddies (around 112°E, 14°N) in the western SCS are periodically and seasonally modulated by monsoon and circulation (Chu et al., 2020), where the probabilities of occurrence of relatively large eddies are approximately 25% (Lin et al., 2007).

The strong eastward jet offshore of Vietnam during southwest monsoon is usually accompanied by a dipole structure with an anticyclonic eddy (cyclonic eddy) south (north) of the jet (Wang et al., 2003). In July and August, an anticyclonic eddy develops to the southeast of the Vietnam coast, transferring the cold coastal water offshore to the SCS interior (Xie et al., 2003). Formation of eddy pairs off eastern Vietnam is a seasonal phenomenon and displays remarkable interannual variability (Chen et al., 2010). The wind, the western boundary current, the eastward jet, and their interaction with topography may influence the generation of eddies off the eastern Vietnam coast (Hwang and Chen, 2000; Xie et al., 2003; Chen et al., 2010). In boreal summer, the summertime eastward jet, as an extension of the Vietnam coastal current, is primarily induced by local wind changes (Li et al., 2014). During northeast monsoon, cyclonic circulation occupies the entire SCS, making the South China Sea western boundary current (SCSwbc) stronger. The monsoon, Luzon Strait transport (LST), and El Niño and Southern Oscillation (ENSO), are all important to regulate SCS circulation and the eddies (Chen et al., 2010; Liu et al., 2011, 2012; Chen and Wang, 2014; Chu et al., 2014, 2017; Lyu et al., 2016; He et al., 2019; Wang et al., 2019, 2020; Zu et al., 2019, 2020).

Energetics analysis is a useful approach to explore the dynamics and mechanisms of ocean eddies. Zhuang et al. (2010) used energetics analysis to evaluate the contributions from instabilities of mean flow to eddy kinetic energy (EKE) in the SCS. Wind stress forces, barotropic/baroclinic instabilities, and pressure gradient together influence the interannual variability of EKE in western SCS (Gan and Qu., 2008; Chen et al., 2009, 2010; Wang et al., 2013a; Chu et al., 2014; Li et al., 2017). Mesoscale variability located offshore of Vietnam (Fig.1, blue box) plays an important role in regulating the SCSwbc by transferring eddy energy. The kinetic

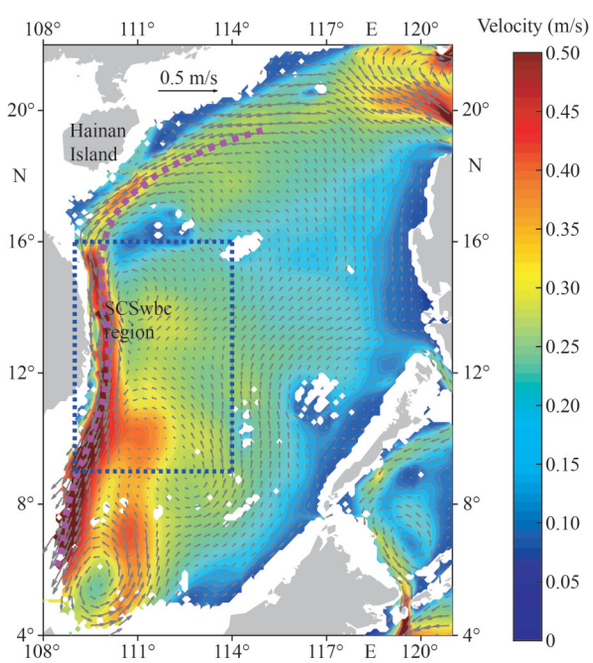

Fig.1 Climatological mean winter sea surface current in the SCS, averaged from December 1993 to December 2017

Shadings represent the magnitude of velocity (unit: m/s) and grey arrows represent the velocity vector. Pink dots indicate the mean SCSwbc jet axis and the blue box is the main study domain (9°N–16°N, 109°E–114°E).

energy pathway reveals that the external forcing dominates upper layer circulation, and the coupling between internal and external dynamics is crucial for maintaining the circulation in middle and deep layers (Cai and Gan, 2021). The SCSwbc is the major component of the SCS throughflow (e.g., Qu et al., 2006; Wang et al., 2006b, 2013a; Fang et al., 2012) and has obvious interannual variability (Fang et al., 2002, 2012; He and Wang, 2009; Wang et al., 2013b, 2016; Zhu et al., 2015; Quan et al., 2016; Li et al., 2017; Zu et al., 2019). Two types of winter circulation exist in the SCS during boreal winter, namely, "O" and "U" (Zu et al., 2019). For pattern "U", the SCSwbc is strong and continuous with large positive vorticity along the isobaths all the way southward forming a strong and unclosed "U" -shaped cyclonic circulation. For pattern "O", the SCSwbc is much weaker with one part continuing to extent southward forming a closed "O" -shaped cyclonic circulation and the other part turns northeast off the coast of Vietnam (Fig.2). The detailed process of energy conversions and their effects on eddy activities are still unclear, and this is the purpose of this study. Exploring the relationship between the SCSwbc and EKE can provide useful insights into the importance of mesoscale activity on

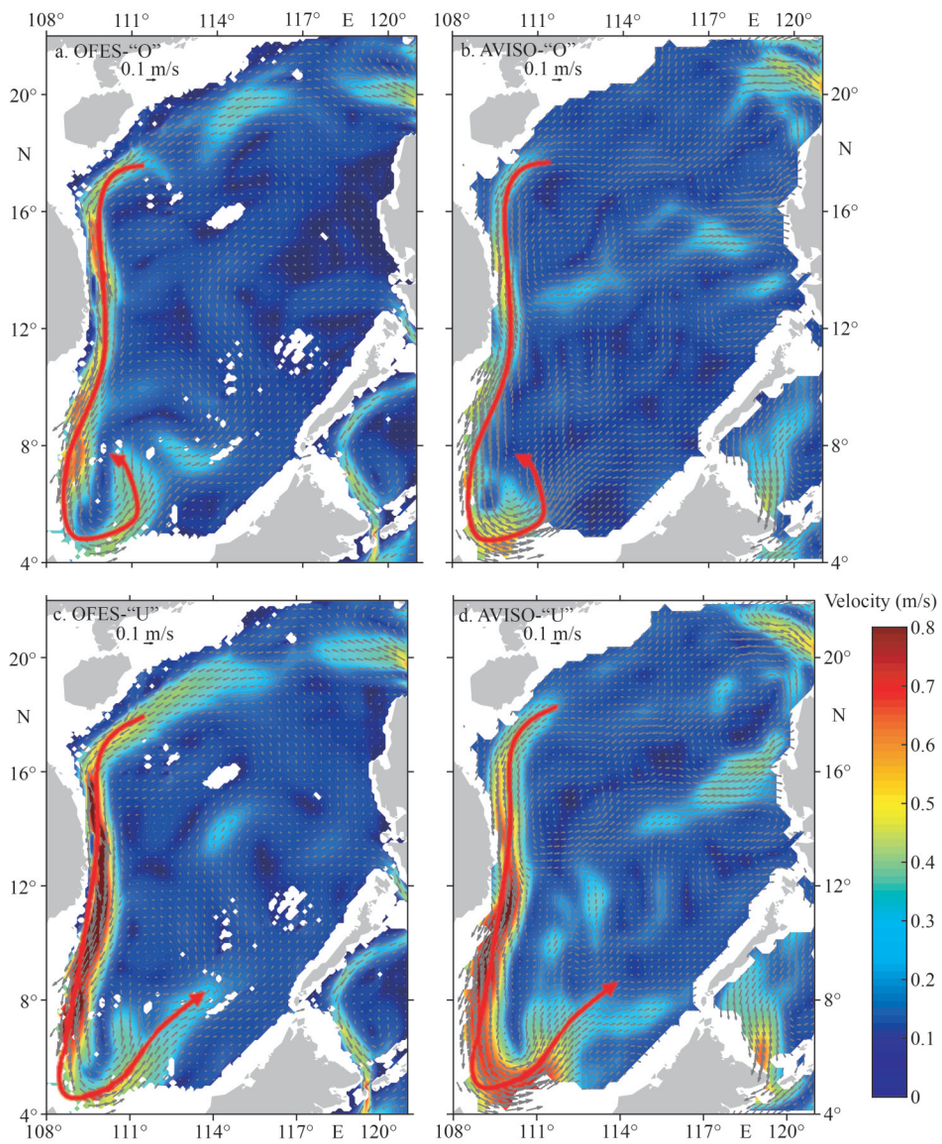

Fig.2 The horizontal distribution of upper layer current from OFES outputs (a, c) and geostrophic current from altimeter data (b, d)

(a–b) and (c–d) for the composite of "O" and "U" years. The gray arrow represents the velocity vector, the color shedding represents the absolute velocity (m/s), and the red bold arrow represents the movement of the western boundary current.

the SCS circulation.

In this study, the interannual variability of EKE and related dynamics in the SCSwbc region associated with two types of winter circulations are explored (Fig.1). The paper is organized as follows. In Section 2, data and methods are introduced. In Section 3, the interannual variability of EKE is presented, including its relationship with ENSO, wind stress forcing, and volume transports. The energy budgets are done in Section 4 to further illustrate the dynamical mechanisms. Finally, the discussion and summary are presented in Section 5.

2 DATA AND METHOD

2.1 Data

The monthly mean outputs of temperature, salinity, and velocity data from the hindcast run of Ocean General Circulation Model (OGCM) for the Earth Simulator (OFES) are used in this study (Sasaki et al., 2004, 2008). Covering the global domain from 75°S to 75°N, the OFES model has an eddy-resolving 0.1°×0.1° horizontal resolution and 54 vertical levels with increasing thickness based on the real ocean stratification. Its high resolution in time and space can adequately capture the mesoscale ocean processes and provide valuable insights for quantifying the energy balance (Zhuang et al., 2010; Qiu et al., 2014; Sun et al., 2016; Zhang et al., 2020). In this study, the model output from January 1993 to December 2017 is analyzed. The Niño3.4 index from 1993–2017 is obtained from the website (https://climatedataguide.ucar.edu/climate-data/nino-sst-indices-nino-12-3-34-4-oni-and-tni).

To validate the OFES simulation in our study domain, some comparisons are done as follows. Firstly, the upper layer current of OFES and the satellite geostrophic current obtained from Copernicus Marine and Environment Monitoring Service (CMEMS) are given in Fig.2. The altimeter data has a 1/4°×1/4° horizontal resolution with daily intervals. To synchronize with the period of the model time, the satellite altimeter data are averaged on monthly basis from January 1993 to December 2017. As shown in Fig.2, the OFES can well capture the horizontal characteristic of the cyclonic circulation in the "U"/"O" pattern respectively. Secondly, we compared the sea surface EKEs (Eq.1) between OFES (using the upper 2.5-m simulation results) and satellite altimeter data (Fig.3). EKE is an important term to indicate the generation and decaying of eddies, and high eddy activities occur near the Vietnam coast. The horizontal distributions of EKEs (Fig.3a–b) indicate that the OFES simulation can adequately capture the basic characteristics of EKEs in our study domain (9°N–16°N, 109°E–114°E; Fig.1, blue box), although it is not ideal and larger than Archiving, Validation and Interpretation of Satellite Oceanographic (AVISO) results in some regions, such as the boundary current system (Feng et al., 2017). By evaluating the standard deviation, the ration of OFES and AVISO is about 1.1 averaged in our study region (Fig.1, blue box). The difference in spatial and temporal resolution of data will have an impact on the magnitude of kinetic energy (KE) (Hu et al., 2020). Only eddies with a radius greater than 25 km could be detected by satellite data (Tuo et al., 2019), and the mesoscale motion is likely to be underestimated due to the resolution of satellite altimeters (Cheng and Qi, 2010; Tuo et al., 2019; Ni et al., 2020; Kubryakov et al., 2021). In addition, we use geostrophic current to calculate the EKE of AVISO, this perhaps is another reason to cause their underestimation. As shown in Fig.2d, we should note that the model exists some discernible biases, especially in region (108°E–111°E, 4°N–8°N), where larger EKEs appear in AVISO. The biases also exist in other regions, such as the Kuroshio intrusion. This discernible bias in the southern SCS could have some impacts to recognize the amplitude of "U" pattern circulation in southern SCS, but will not substantially change the results in the study area (Fig.1, blue box) in this paper. In general, the model results to a little underestimate of the current amplitude (Wang et al., 2013b), mostly because of the artificial smooth and diffusion existing in model simulation. The large EKE is found in AVISO around the Kuroshio intrusion (Fig.3a–b), and this perhaps implies that the Kuroshio currents of OFES is underestimated and thus the simulated Kuroshio's intrusion is weakened. Sensitivity study reveals that the weakening of the Kuroshio markedly enhances Kuroshio's intrusion (Gan et al., 2006). Figure 3c shows the time series of area-averaged EKEs calculated from two datasets, and their correlation coefficient can reach 0.54 (for a simple statistical analysis, we assume the sample number is 25, and therefore r_α=0.396, with 95% confidence level; r_α= 0.337, with 90% confidence level). Previous studies also showed that the OFES does a reasonably good job in simulating the circulation and EKE in the SCS (Sun et al., 2016). By evaluating the model and satellite data, the model can basically capture the pattern and EKE activity shown in satellite data,

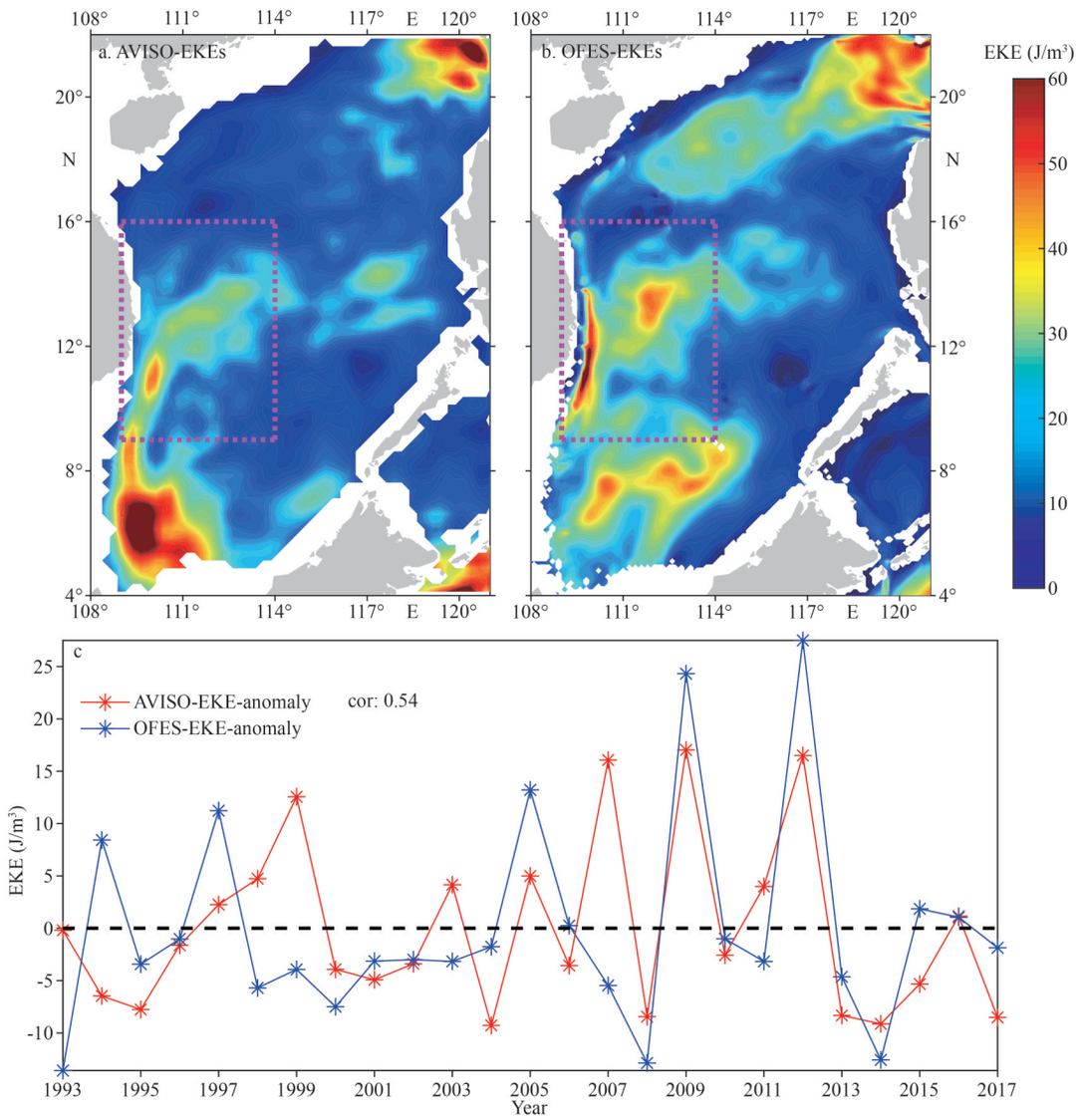

Fig.3 Horizontal distribution of mean sea surface EKE (unit: J/m³) in December calculated from AVISO data (a), OFES model outputs (b); time series of box-averaged EKE in December from 1993 to 2017 (c)

Pink dot box represents the main study domain consistent with Fig.1. "cor: 0.54" represents the correlation coefficient of EKE calculated from AVISO and OFES is 0.54.

especially for winter circulation in study region. Thus, we believe the OFES data are suitable to be used in this study for investigating the interannual variability of EKE and quantitative analysis.

Generally, the basin-scale cyclonic circulation can exist for approximately 2–4 months from November to February next year (not shown). However, the strongest development of cyclonic circulation occurs in December (Zu et al., 2019). To ensure consistency with the previous study by Zu et al. (2019), we also adopted data for December (i.e., the mature stage) to study the interannual variability of winter circulation in the SCSwbc domain. Both the EKE and wind energy reach their maximum in December–January (Yang et al., 2013). Considering that the tides and internal waves are strong in the continental shelf, data shallower than 100 m are omitted.

2.2 Method

The expression of EKE is as follows:

$$EKE=1/2\ \rho_0(u'^2+v'^2). \quad (1)$$

Here, (u, v) is horizontal velocity and prime ("()'") represents the deviation from the time-mean, ρ_0=1 025 kg/m³ is the constant reference density. Mechanisms responsible for eddy activity can be quantified by EKE energy budget, including the terms of the internal exchange between the mean

and eddy kinetic energy, the exchange with potential energy, and the external energy from wind stress et al. (Eq.2). Following the work of Ivchenko et al. (1997), the EKE budget equation is given as follows:

$$\frac{\partial \mathrm{EKE}}{\partial t} = \underbrace{-\rho_0\left(u'u'\frac{\partial \bar{u}}{\partial x} + u'v'\left(\frac{\partial \bar{v}}{\partial x} + \frac{\partial \bar{u}}{\partial y}\right) + v'v'\frac{\partial \bar{v}}{\partial y}\right)}_{\mathrm{BTC}} - \underbrace{g\rho'_* w'}_{\mathrm{VEDF}} + \underbrace{u'\tau'_x + v'\tau'_y}_{\mathrm{WW}} - \underbrace{\left(u'\frac{\partial P'}{\partial x} + v'\frac{\partial P'}{\partial y}\right)}_{\mathrm{PW}} - \underbrace{\left(u\frac{\partial \mathrm{EKE}}{\partial x} + v\frac{\partial \mathrm{EKE}}{\partial y} + w\frac{\partial \mathrm{EKE}}{\partial z}\right)}_{\mathrm{ADV}} + \mathrm{DIFF}, \quad (2)$$

where $\frac{\partial \mathrm{EKE}}{\partial t}$ is the time change of EKE. On the right side of Eq.2, the first term BTC is the work of Reynolds stress against the mean shear, and it represents the energy transfer from mean flow to eddy energy, which, if positive, indicates the occurrence of barotropic instability; the second term VEDF represents the baroclinic conversion through vertical eddy density flux from eddy potential energy (EPE) to EKE; and the third term WW indicates the generation of EKE by wind input, which is associated with the time-varying surface wind forcing and ocean circulation. PW and ADV represent the redistribution rates of EKE through pressure work and ocean advection, respectively, and the last term DIFF is the residual, including the deviation of model simulation, the error caused by the selection of calculation depth, dissipation due to viscosity, and diffusion. It is difficult to directly calculate the DIFF term accurately, and therefore, it is not considered in this study.

Here, (u, v, w) is the three-dimensional velocity, P is pressure, ρ is density, τ_x, τ_y is zonal/meridional components of the wind stress, g is gravitational acceleration. The overbar ("$\overline{()}$"') denotes the time-mean, and prime ("()'") represents the deviation from the time-mean and indicates transient eddy terms; $\rho_* = \rho - \rho_r$ is the perturbation density, and ρ_r is the background density field averaged over the study area (Fig.1, blue box) and period (from December 1993 to December 2017). Figure 4 clearly illustrates the expression of Eq.2. Notably, $\frac{\partial \mathrm{EKE}}{\partial t}$ is hard to be fully balanced with terms in the right side of Eq.2 because of adjustments applied when simulating data, and implies that the residual terms omitted here are important to balance the EKE equation. In addition, positive terms on the right side of Eq.2 can represent energy inputs to EKE; however, negative terms cannot completely represent the outputs of EKE. Calculation of the energy budget for open regions is complex but can provide useful information about its relative importance. In the following discussion, in case of no special statement elsewhere, EKE signifies the integration in upper 241 m, and the map of the ocean current signifies the vertical average in upper 241 m.

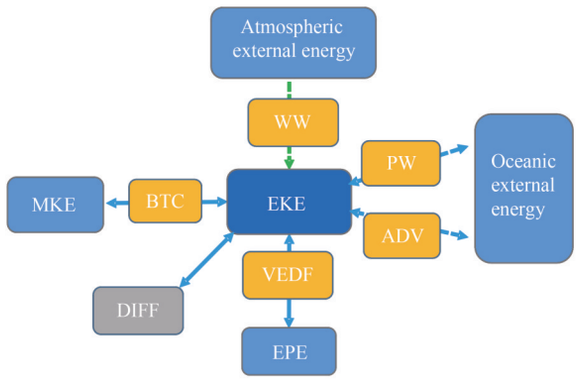

Fig.4 The EKE energy balance

Solid arrows indicate the energy conversion within the local ocean domain, and dashed arrows illustrate the external forcing of EKE outside the local ocean domain.

3 RESULT OF EKE VARIABILITY

3.1 Mean EKE distribution in the winter season

Figure 5a illustrates the mean horizontal distribution of EKE integrated in the upper 241 m, which is averaged in December from 1993 to 2017. Northeast monsoon first appears over the northern shelf in October, and then expands southward, and reaches its maximum in December (Xue et al., 2004). Therefore, the basin-scale cyclonic circulation in the winter season is well developed in December, and as a result, a significant EKE center is present in western SCS, with a high value (>7×10^3 J/m^2), limited off the Vietnam coast as a narrow strip and extended southward starting from 14°N. The vertical profiles of EKE after being averaged in the longitude and latitude direction within the study area are shown in Fig.5b–c. The EKEs are largely concentrated in the upper 241 m (Fig.5b–c) and rapidly decays from the surface toward deeper ocean, with the highest value located at 110°E, 13.5°N–14°N. Considering that the eddy energy in the SCS is confined to the upper layer (Li et al., 2017; He et al., 2018), only the upper 241 m of the water column are examined in

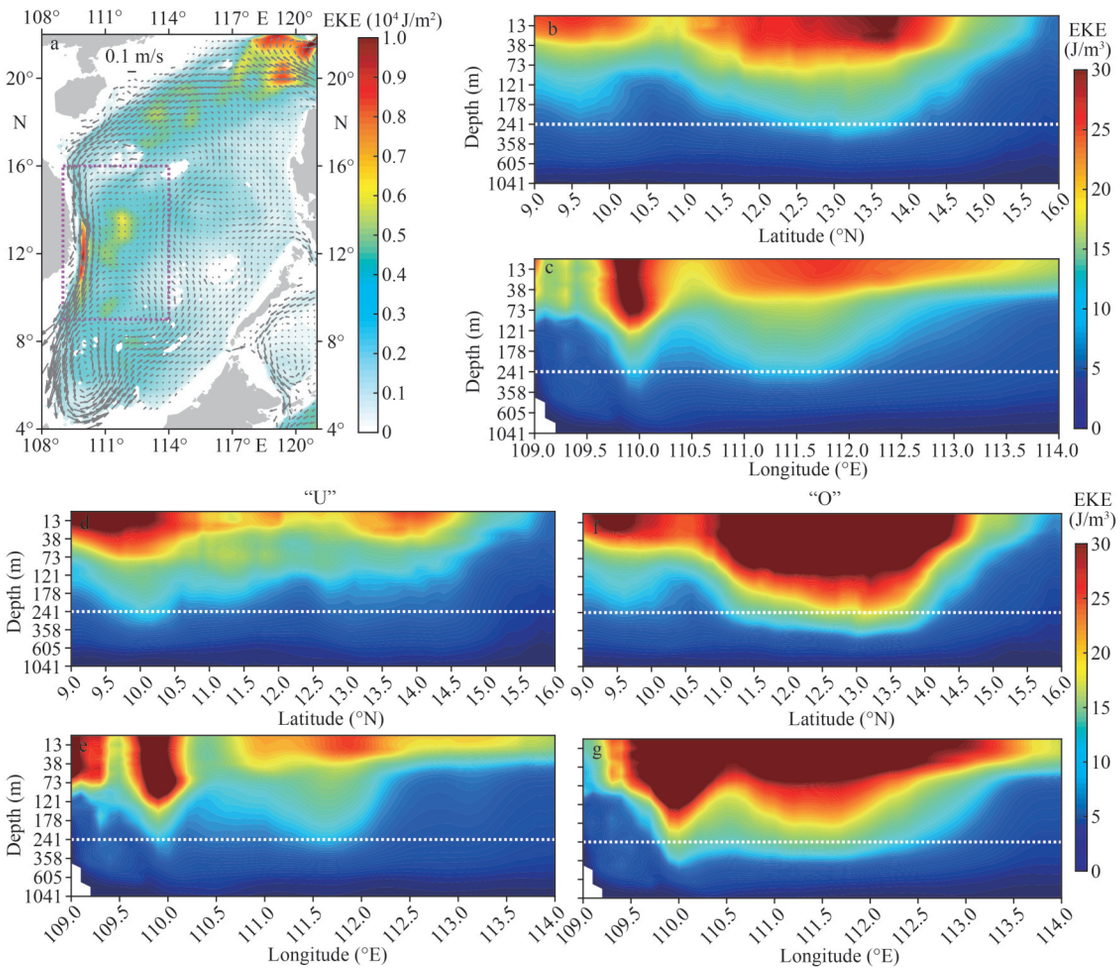

Fig.5 Horizontal distribution of the integrated EKE (colors, unit: 10^4 J/m^2) in upper 241 m (a); vertical profiles of EKE (unit: J/m^3) after the zonal (9°N–16°N) and meridional (109°E–114°E) averaging (b & c); (d–e, f–g) as same as (b–c) but for pattern "U" and "O" respectively

The vertical average ocean currents are superimposed (vectors). Both EKE and ocean current are time-averaged in December from 1993 to 2017. The white dotted line is 241 m.

this study, which is much shallower than that in Kuroshio region (800 m or deeper, e.g., Yang et al., 2013; Geng et al., 2016; Sun et al., 2017). The results show that the vertical differences are obvious discernible for two types winter circulation events (Fig.5d–g). When the SCSwbc is strong associated with "U" patterns (Fig.5d–e), the EKE is confined along the coastal areas and offshore energy is much weaker than climatological mean. But for pattern "O", the peak of EKE extends much deeper and far away from the coastal areas when the SCSwbc decreases (Fig.5f–g), indicating the energy transferring from mean flow to eddy activity.

The variance of the altimeter measurements of sea surface height (SSH) shows that the region off the coast of central Vietnam is a dynamic active area (Ho et al., 2000), which indicates that the eddy energy in this region is strongly connected with upper layer circulation related to the wind stress forcing, Kuroshio intrusion, and some other factors, such as topography. In winter, a stronger cyclonic gyre exists in the western SCS, and the boundary current strengthens, corresponding to strong off-shelf northward upwind flow (Natuna off-shelf current) (Fang et al., 2002), and then, the mesoscale eddies in this region become active.

3.2 Abnormal EKE variability and its relationship with Niño3.4

To explore the relationship among EKE, KE, and ENSO events in the SCSwbc region the empirical orthogonal function (EOF) analysis of the monthly mean kinetic energy (KE=$1/2\rho_0(u^2+v^2)$) and EKE in December was performed. The method of EOF

analysis involves the decomposition of a signal or data set in terms of orthogonal basis functions. The EOF analysis can provide the eigenvectors and eigenvalues of the spatial covariance matrix of a dataset, representing the spatial characteristics of oceanic variability and time variability. The spatial pattern and the principal component of the first EOF mode (PC1) of EKE are shown in Fig.6a–b, respectively. The leading EOF mode shows that large EKE magnitude exists off the Vietnam coast, especially along the SCSwbs (Fig.6a) where large variance is concentrated, which is consistent with the dynamic active area of Ho et al. (2000), and PC1 can explain approximately 37.2% of the total variance of EKE. Figure 6b–c represents the PC1 of EKE and KE (the horizontal distribution is not shown), and as shown in the figure, both KE and EKE in the winter season have significant interannual variabilities. The horizontal distribution and time series of leading EOF modes of EKE and KE inferred from OFES outputs have been compared with those from AVISO data, and results are basically similar (not shown). Of course, we should keep in mind that there are some discernible differences exist between OFES and AVISO. As pointed in Fig.3, the OFES EKE is stronger than observation in boundary current, with stronger interannual variations. Therefore, an obvious high-value center occurs in the nearshore area (Fig.6a). The EKE is larger than AVISO results in the boundary current system, indicating that the boundary current will be overestimated in OFES model.

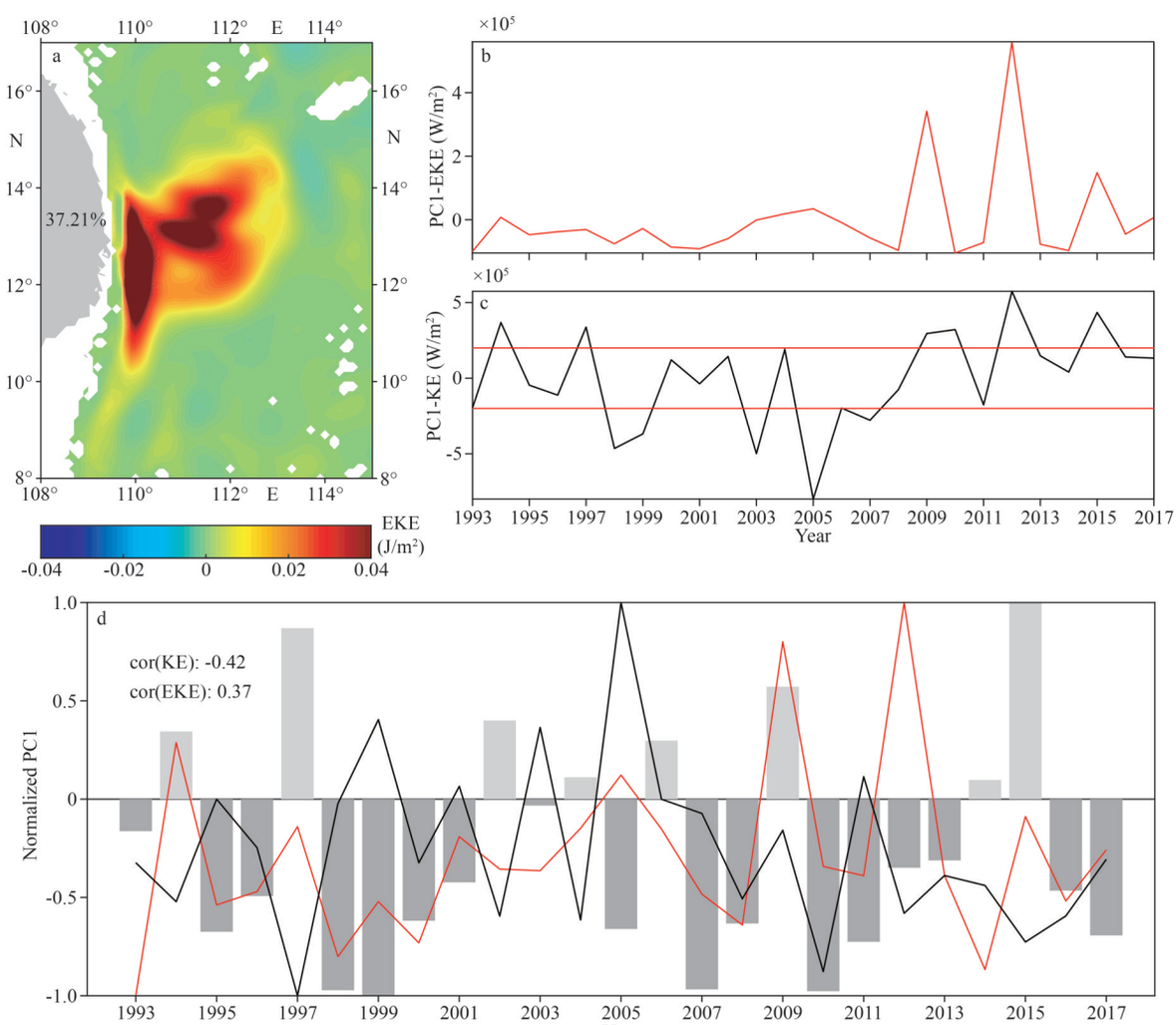

Fig.6 Leading EOF mode of EKE off Vietnam coast (a); principal components of the first mode (PC1) of EKE and KE respectively (b–c); normalized time series of EKE (red line) and KE (dark line) anomalies averaged in the study domain (d)

Niño3.4 index is superimposed (bar). "cor(KE)/cor(EKE)" represents the correlation coefficients between KE/EKE and Niño3.4.

Following the method of Zu et al. (2019), years with larger variabilities of KE PC1 are selected to do a composite analysis (Fig.6c). The "O" type winter circulation includes 1994, 1997, 2009, 2010, 2012, and 2015 (PC1 larger than 2×10^5); the "U" type winter circulation includes 1998, 1999, 2003, 2005, 2006, and 2007 (PC1 smaller than -2×10^5). The remaining years are defined to be normal years. We found that these years during "O" and "U" type winter circulation have a certain relationship with ENSO events. The relationship between winter circulation with "O" and "U" patterns and ENSO can be depicted in Fig.6d. The Niño3.4 index is negatively/positively correlated with KE/EKE evolution in SCSwbc (correlation coefficient=-0.42/0.37, exceeding 95% and 90% confidence level), indicating that ENSO plays a role in causing EKE variability in this region (Chen et al., 2009, 2010; Zhuang et al., 2010; Chu et al., 2014, 2017).

Figure 7a–b presents the horizontal distributions of EKE (vertical integrated in upper 241 m) and corresponding ocean circulation superimposed with flow field in patterns "U" and "O", respectively. In pattern "U", remarkably strong SCSwbc with cyclonic circulation exists along the coast of Vietnam, and an unclosed cyclonic circulation forms along the southern continental shelf (Fig.7a). Half of the composite years for pattern "U" are in the early or mature stage of La Niña events, such as 1998, 1999, and 2007. In pattern "O", SCSwbc is diverged around 13°N and forms a two-branch structure, with one part continuing to extend southward and the other part deflecting eastward (Fig.7b). The SCSwbc in "O" year is much weaker so that the cyclonic circulation in the south of SCS could develop into a closed gyre (Fig.7b), and most of the component years are in the mature stage of El Niño events, such as 1994, 1997, 2009, 2015. Compared with pattern "U", the boundary current in pattern "O" is significantly weakened, and the difference in EKE (Fig.7c) mainly occurs in the eastern region of boundary current (12°N–14°N).

To determine the difference in EKE between the two types of winter circulation, the time series of

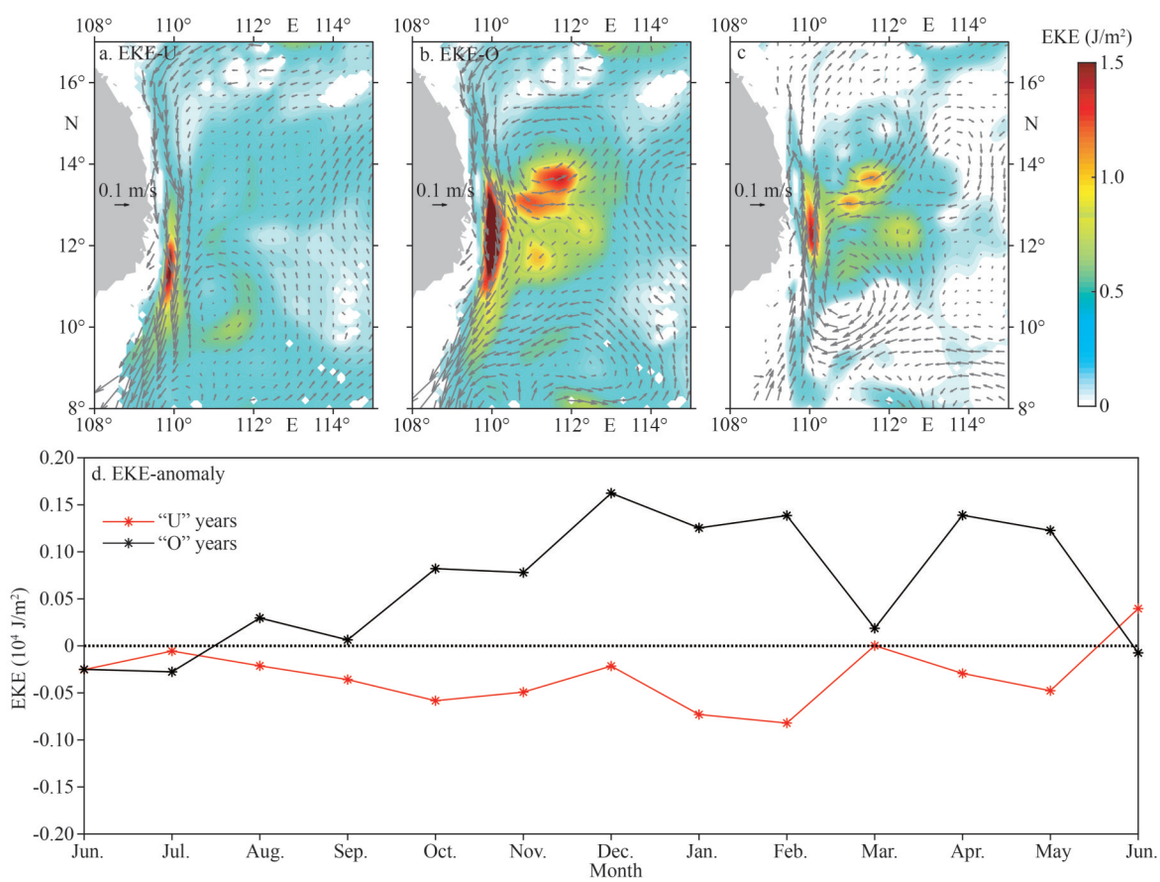

Fig.7 Composite current and EKE in pattern "U" (a), pattern "O" (b), and the difference between the two patterns "O" minus "U" (c); time series of EKE anomaly in pattern "U" (red line) and pattern "O" (dark line) from June to the following June (unit: 10^4 J/m²) (d)

EKE anomaly was averaged in the study domain from June to the following June, as shown in Fig.7d. The anomalies in Fig.7d are calculated in the formula:

$$E_{Ua}(t)=E_U(t)-E_m(t), \quad (3)$$

$$E_{Oa}(t)=E_O(t)-E_m(t), \quad (4)$$

where E represents EKE in Fig.7d and each term in Eq.2; E_m represents the average from Jan. to Dec. in 25 years; E_U/E_O represents the average from Jan. to Dec. in "U"/"O" composite years; E_{Ua}/E_{Oa} represents the anomalous values relative to the climatological mean results in the corresponding month.

The EKE anomaly is significantly different in two types of circulation, corresponding to a negative/positive EKE anomaly in pattern "U"/"O" winter circulation. It can be found that during the mature stage of El Niño events, SCSwbc decreases and EKE increases, while the impact of La Niña events is much weaker than that of El Niño events (Figs.6–7). Previous studies have pointed out that ENSO events can affect EKE and the upper layer circulation in SCS to some extent. ENSO can affect the SCS regional wind, and therefore affects the SCS circulation and eddy activities (Xiu et al., 2010). The interannual variation of local wind stress curl associated with ENSO events may be the cause of the interannual variation of the EKE in the SCS (Chen et al., 2009; Cheng and Qi, 2010). However, the ENSO events do not perfectly coincide with the years of "O" and "U", indicating that in some years, some other factors to regulate the variation of EKE in SCSwbc region rather than ENSO events.

3.3 Relationship among EKE, SCSwbc transport, and wind stress forcing

The observation results show that the volume transport in the north of the SCS (NSCS) was affected by the mesoscale eddies (Zhu et al., 2015). When the transport of NSCS is minimum (maximum), a cyclonic (anticyclonic) eddy would extend to the southeast side of the observation line, and then induce a southwestward (northeastward) transport anomaly. The large EKE along the slope in the simulation extends into the SCS which means the stronger Kuroshio intrusion in the simulation (Fig.3b). Furthermore, the wind stress is an important factor regulating the SCSwbc in the winter season (Quan et al., 2016), in addition to the role of Kuroshio intrusion. As the relationship between EKE and SCSwbc transport and wind stress forces will be investigated in this section, the volume transport through section (12.5°N, 109°E–114°E) integrated in upper 241 m is selected to represent SCSwbc transport in the upper ocean. In addition, it is necessary to discuss the possible impacts of Kuroshio intrusion on SCSwbc. The Luzon Strait transport is calculated to simply represent the Kuroshio intrusion.

Figure 8a gives the time series of Luzon Strait transport vertically integrated along the section (121°E, 17°N–23°N). The time-longitude section of meridional velocity anomaly shows that the modelled strongest SCSwbc is mainly limited in west of 110.5°E (Fig.8b), and this southward current can extend to a depth of ≥800 m (Fig.8c–d), which is consistent with observational evidence (Guo et al., 1985; Zhou et al., 2010). Seen from Fig.8a–b, in general, in the "O" years, the Kuroshio intrusion is relatively weak, corresponding to the weakening of the SCSwbc; while in the "U" years, the Kuroshio intrusion is strong, corresponding to the strengthening of SCSwbc The observed SCSwbc in the Xisha area flows southwestward above 450 m from November to April, with a maximum velocity of >60 cm/s (Shu et al., 2016). The SCSwbc transport in the central part of the coast of Vietnam reaches its maximum value in winter and has obvious interannual changes (Quan et al., 2016). Thus, in "U" and "O" years, the composite fields of southward meridional velocities are abnormally enhanced or weakened (Fig.8c–d). Furthermore, there are significant interannual changes in the SCSwbc structures, including position, width, and maximum depth (Quan et al., 2016), partially reflected in Fig.8b. Compared with the U-shape, the main axis of the O-shape apparently extends eastward. Figure 8a–b also reflect that the strong-weak-strong decadal variations of LST and SCSwbc.

The SCSwbc in winter is mainly attributed to the monsoon and Kuroshio intrusion (Chen and Xue, 2014). Numerical experiments confirmed that a reduced Kuroshio intrusion could slightly reduce mesoscale activities in the northern SCS, but the EKE variability in the southwest SCS cannot be directly explained by Kuroshio intrusion alone (Feng et al., 2020). Quan et al. (2016) found that the wind forcing makes a primary contribution to the interannual variability of the winter SCS WBC, whereas the influence of Kuroshio intrusion is secondary.

Red and blue arrows represent the years of "O" and "U" patterns, respectively; positive indicates eastward/northward.

To explore the relationship among advection

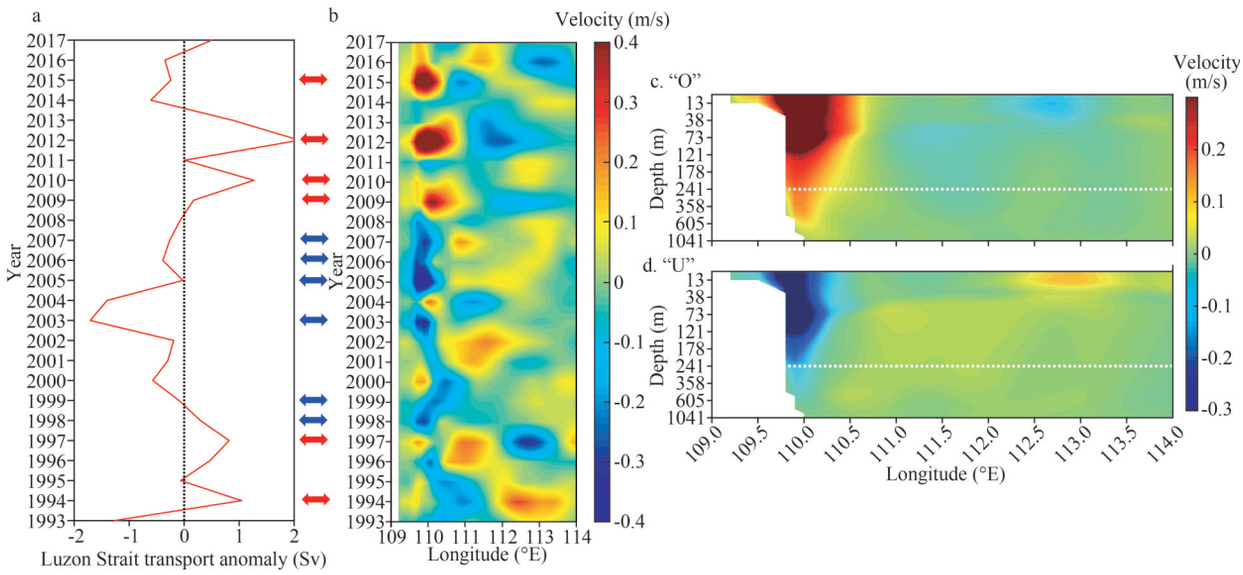

Fig.8 The time series of Luzon Strati transport anomaly (eastward is positive) (a); time-longitude section of meridional velocity anomaly (m/s) along 12.5°N (b), composite vertical meridional distribution of the meridional velocity anomalies in "O" and "U" pattern years (c–d), respectively, at the 12.5°N section

The red/blue bidirectional arrow between (a) and (b) represents the "O"/"U" years.

transport, wind stress, and EKE under different circulation patterns, the mean state and the anomalies of wind stress (WSA) and wind stress curl (WSCA) in the "U" and "O" years are shown in Fig.9a & c, respectively. At the same time, the mean state and the anomalies of volume transports (TSA) of three sections in the study area are superimposed. Clearly, the WSA deflected to the northeast in the "O" year, and the WSCA was negative in a large area. The transport anomalies through 9°N and 16°N are northward, which indicates that the southward SCSwbc is weakened under the abnormal northeast monsoon forcing in the "O" years, and vice versa in "U" years. Figure 9d shows the time series of EKE, 12.5°N TSA, and WSA in winter. The correlation coefficient between EKE anomaly and TSA (WSCA) is 0.70 (-0.40), both exceeding 95% confidence level. And the correlation coefficient between TSA and WSCA is -0.63, exceeding 95% confidence level. Under the abnormal south-westward wind stress force, the southward transport in SCSwbc increases with Ekman detrainment, corresponding to the abnormally weakened EKE in "U" type years. However, in "O" type years, the southward transport in SCSwbc decreases with Ekman entrainment, corresponding to the abnormally strengthened EKE. The local wind stress curl plays an important role in the interannual variability of the eddy, and the eddy activity is related to the strength of the background flows (Chen et al., 2010, 2011). Sun and Lan (2021) pointed out that in the summer season, the response of SCSwbc to El Niño could be attributed to the setting up of the anticyclonic circulation in Sverdrup balance driven by the negative wind stress curl in the southern SCS. Thus, the response of SCSwbc in "U"/"O" years can also be explained by the setting up of the abnormal cyclonic/anticyclonic circulation in Sverdrup balance driven by the abnormal positive/negative wind stress curl, respectively.

This abnormal wind stress curl can exert either a direct effect on the regulation of the interannual variability of EKE or an indirect way by changing the SCSwbc transport (Zu et al., 2019). The local wind stress curl is also a dominant driving force to spin up the mesoscale eddies in the eastern SCS and then spread westward (Wang et al., 2008b). The abnormal transport in western SCS can also be attributed to the geostrophic current associated with the sea level pattern, which is primarily induced by local wind changes associated with the ENSO (Li et al., 2014). During the development of ocean eddies, the mean current will transfer energy to eddies through the energy conversion process, such as barotropic and baroclinic instability (e.g., Feng et al., 2005). The detailed process of energy conversion in SCSwbc in the summer season was examined by Li et al. (2017) and Yao et al. (2017). In Section 4, we further discuss how the wind stress and energy conversion inside the ocean affects EKE through the energy budget equation.

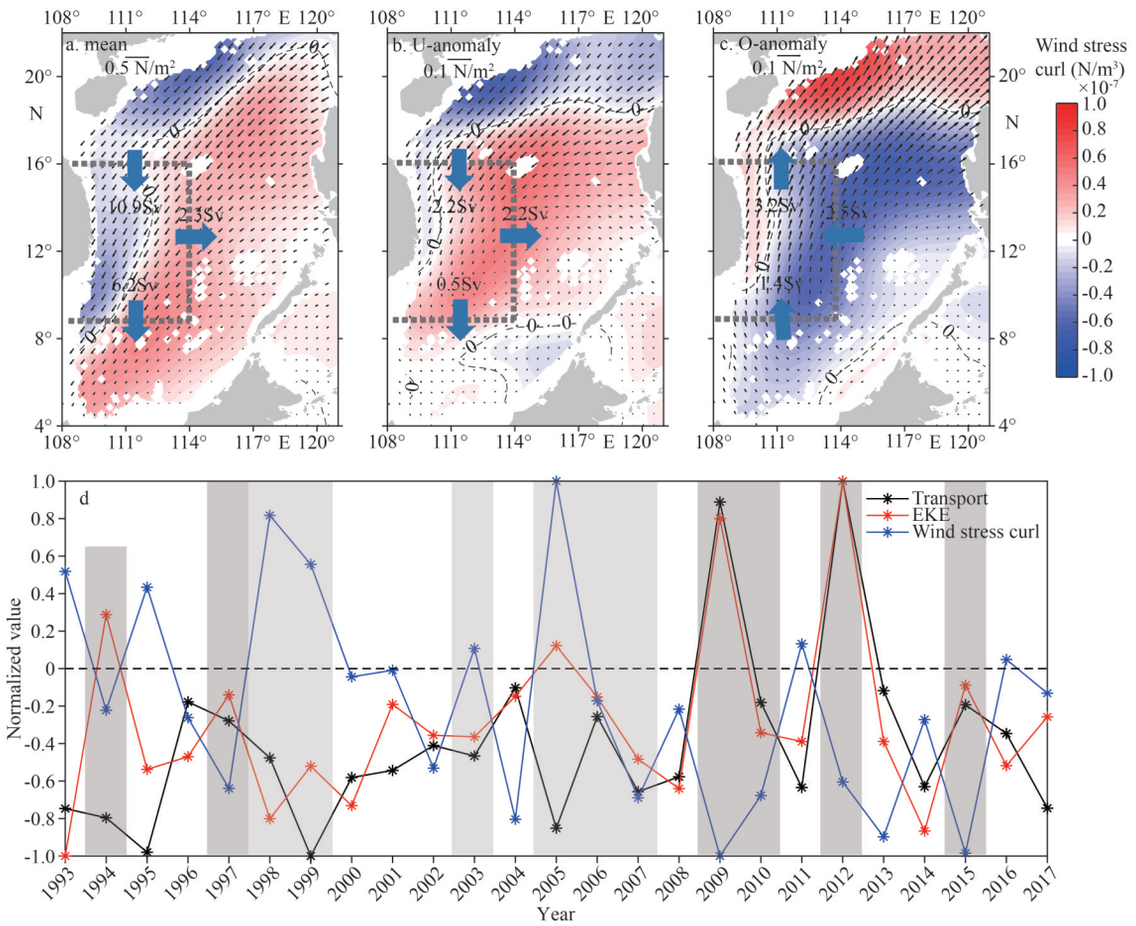

Fig.9 Horizontal distribution of wind stress (arrows) and wind stress curl (shading colors)

a. mean valuse; b-c. anomalies in "U" and "O" years. The dashed gray lines represent the three sections (9°N, 108°E–114°E; 16°N, 108°E–114°E; 114°E, 9°N–16°N), and the numbers on them represent transport on each of the three sections. The numbers and blue arrows indicate the amplitudes and directions, respectively, of volume transport anomalies along three sections; d. normalized time evolution of SCSwbc transport anomaly (black line, positive is northward), box-averaged EKE anomaly (red line), and wind stress curl anomaly. Light and dark shades indicate "U" and "O" years, respectively.

4 ENERGY BUDGET ANALYSIS

4.1 Horizontal and vertical distribution

Horizontal distribution of each term anomaly in Eq.2 corresponding to "U"/"O" pattern is given in Fig.10. By comparing Fig.10a with Fig.10g, it can be found that in pattern "U", the high value of ADV is mainly concentrated in the narrow strip along the Vietnam coastal area and decreases rapidly on the east side of the SCSwbc. In pattern "O", the ADV is negative on the west side of the SCSwbc and positive on the east side and extends eastward to 114°E. The horizontal distribution of mean advection term is heterogeneous and mainly presents negative values (not shown), which is consistent with the findings of Yang et al. (2013).

The mean BTC exhibits a cross-stream variation along coast locations, where negative values are noted on the inshore shallower side of the SCSwbc, while positive values are noted on the offshore side (not shown). The positive values offshore side indicate that the eddy can draw energy from the SCSwbc by barotropic instability. The whole positive BTC anomalies located in the offshore coast of Vietnam in pattern "O" rather than "U" (Fig.10b & h) indicate that the MKE is more easily converted to EKE in pattern "O" through the barotropic instability process.

The VEDF anomalies in "U" and "O" years mainly show an alternating positive-negative pattern (Fig.10d & j), which is mostly confined to the coastal areas of Vietnam. The mean alternating positive-negative pattern of VEDF along the Vietnam coast (not shown) is similar to that in the Kuroshio extension region (Geng et al., 2016) and represents the EKE production due to baroclinic instability. From the horizontal direction, the intensity of VEDF

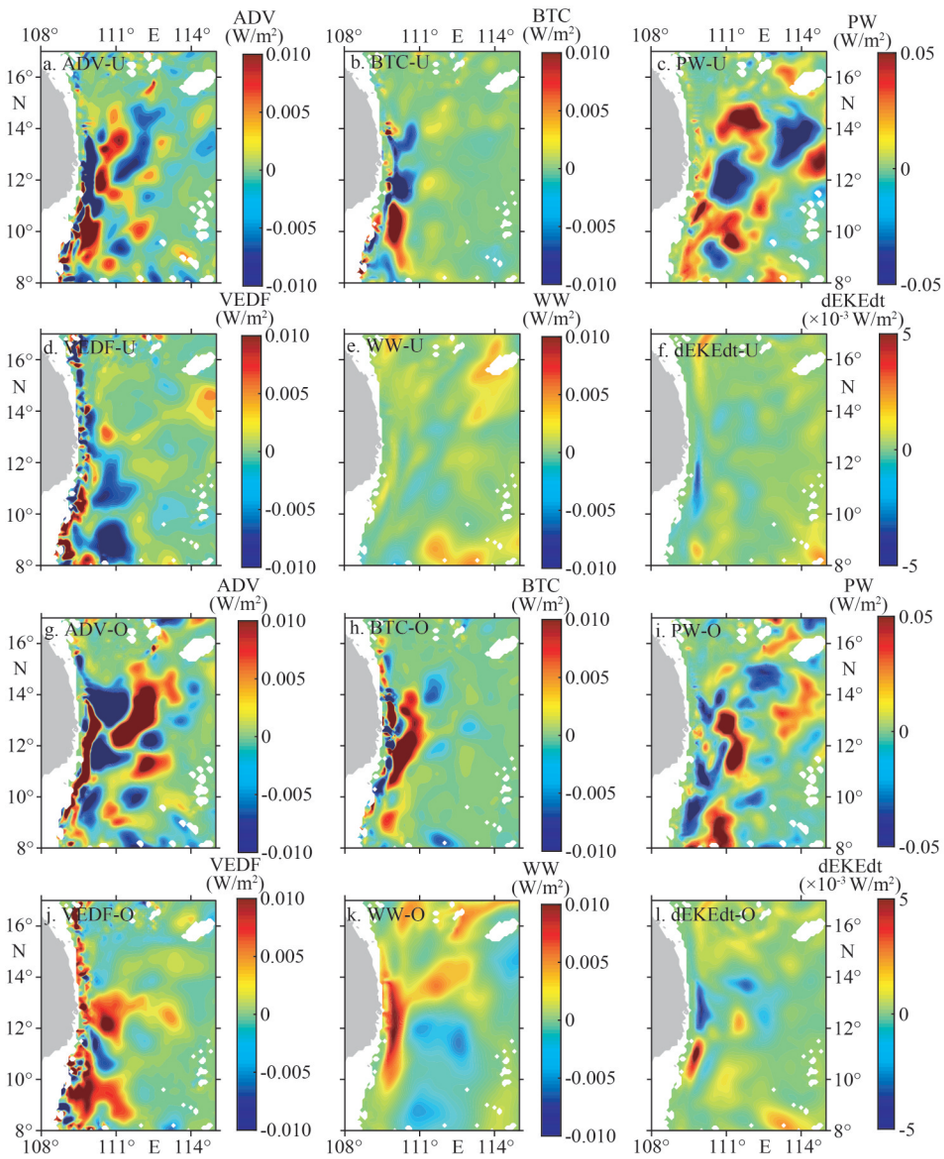

Fig.10 Horizontal distribution of each term anomaly in Eq.2 corresponding to "U" pattern (a–f), and "O" pattern (g–l) (unit: W/m²)

is small comparing to PW and ADV. Because the VEDF fluctuates vertically (Fig.11), the horizontal distribution of VEDF could be cancelled after vertical integration. However, from the perspective of vertical direction and quantitative analysis, VEDF significantly affected the interannual variation of EKE. The detailed analysis will be made in the following part.

Previous studies have confirmed that the wind field exert vital impact on the upper layer circulation of SCS in the forms of wind stress and wind stress curl, especially in the coastal areas of Vietnam (Fang et al., 2002; Gan and Qu, 2008; Lyu et al., 2016; Zu et al., 2019, 2020). The influence of atmosphere is an important factor for regulating the boundary current and eddy activities in SCS. Therefore, we treat the process that the wind field modulating SCSwbc and further influencing EKE as the 'indirect process', while the process that the wind field regulating EKE through WW is the 'direct process'. Figure 10e & k shows that a high WW value is concentrated in SCSwbc, WW was significantly weakened in pattern "U" years, and it was significantly enhanced in pattern "O" years (Fig.10e & k). Combined with Fig.9 & 10, the results indicate that the BTC and WW are both important factors to regulate the EKE variability in "U" and "O" years. In general, under strong winter

monsoon forcing in “U” years, the SCSwbc become strong and the basin-scale cyclonic circulation is fully developed, the BTC from the MKE to EKE and the direct wind input (WW) are both weak, therefore, the EKE is weak and narrowed along the axis of SCSwbc. The situation is reversed for “O” years.

Although the amplitude of time change of EKE is smaller than the other terms, perhaps caused by factors such as sample interval, diffusion, and other uncertainties, the aforementioned results show that the ADV, BTC, and WW either increased or decreased, corresponding to the EKE variability. The underlying variable bottom topography plays an important role in regulating the mean flow pathway and influencing the eddy-mean flow interaction (Ducet and Le Traon, 2001; Gan and Qu, 2008; Hurlburt et al., 2008). It also suggests that the SCSwbc is mainly barotropic unstable in the upper layer. The density of the deep ocean is relatively uniform, and thus, small perturbations of density are likely to cause baroclinic instability in the deeper layer. As the main factor of external energy input of EKE, as same as the summer season (Li et al., 2017), the spatial distribution of PW shows unobvious regularity.

To gain better understanding of the contribution of each term to the interannual variation of EKE at different depths, the vertical distributions of the box-average energy budget are further given in Fig.11 (except for WW). The strongest energy conversions occur at 60 m (Fig.11a), except the PW term extending to the deeper layer of 200 m. For the mean BTC, the positive values indicate that the energy is transferring from MKE to EKE, while the negative values do not mean the reversed conversion process from EKE to MKE (Kang and Curchitser, 2015). For the mean, the strong barotropic instability always occurs at a depth of 30–130 m in the SCSwbc region (Fig.11a, red line), and the difference in BTC anomaly associated with the two patterns is obvious (Fig.11b–c, red lines), indicating its significant role in regulating the interannual variability of EKE in the region of SCSwbc. The positive BTC anomaly implies that the energy is transferring from MKE to EKE in “O” years to contribute to the abnormal strengthen of EKE. Terms of ADV and PW always represent the negative feedback process to EKE in study domain. PW always depresses the kinetic energy in the study domain. VEDF is another term significantly influencing the regulation of EKE variability (Fig.11a, red dashed line). The VEDF reverses between surface and subsurface and has totally different fluctuations in “O” and “U” patterns. The vertical profile of VEDF indicates the eddy density fluxes from EPE to EKE have a significant different role to regulate the EKE change in two patterns and implies that the potential energy is more easily released to kinetic energy in the subsurface (below 60 m) in “O” years by baroclinic instability.

The EKE exchanges energy with the external ocean environment through PW and ADV, which changes significantly on the spatial scale. As shown

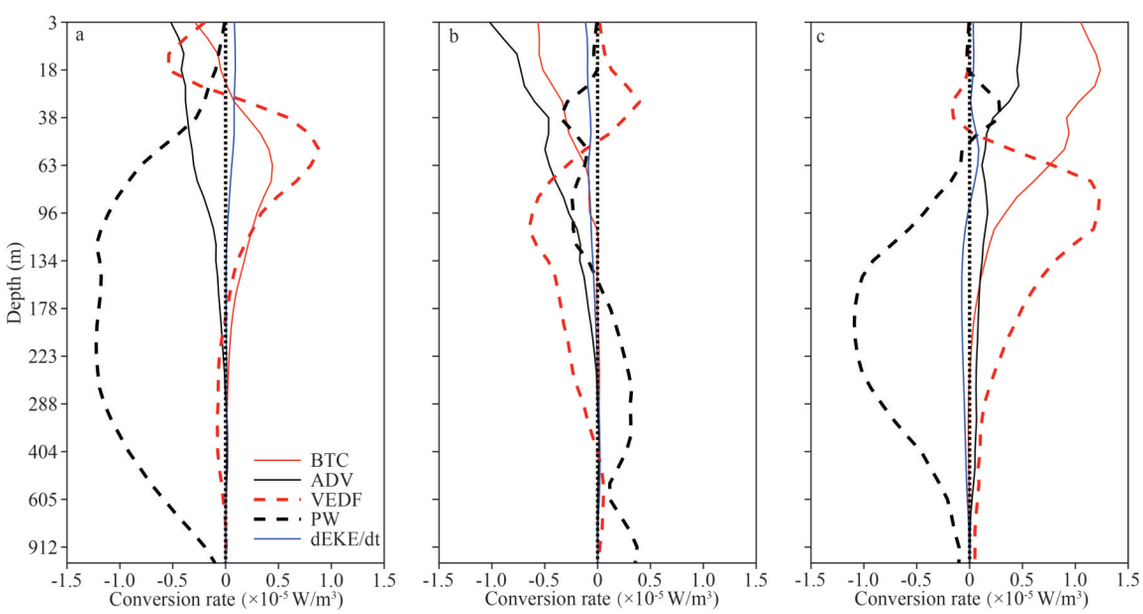

Fig.11 Vertical distribution of box-average each term (unit: ×10^{-5} W/m^3) in Eq.2 (except WW)

a. mean value; b. anomalies in “U” years; c. anomalies in “O” years.

in Fig.11 (black dotted line and the black solid line), PW and ADV are found to work together as the most important sources of transferring EKE to the outside of study domain. PW is predominantly negative in two composite years, offsetting the increase of EKE induced by other terms, while ADV is mainly negative in the mean state and pattern "U" and slightly increased in pattern "O".

4.2 Time evolution and box-average

For further understanding the process of controlling EKE variability corresponding to two types of circulation in the SCSwbc region, the time evolution of area-averaged energy budget analysis and the comparison between two-type circulations are presented in Fig.12. The wind mostly affects EKE by regulating the ocean current through changing the shear of upper layer currents (Yang et al., 2013; Zheng et al., 2018). In winter, the wind stress transfers energy from the atmosphere to the ocean in two patterns (Fig.12a–b, blue lines; Fig.12d, cyan bar). And the MKE continuously transfers energy to

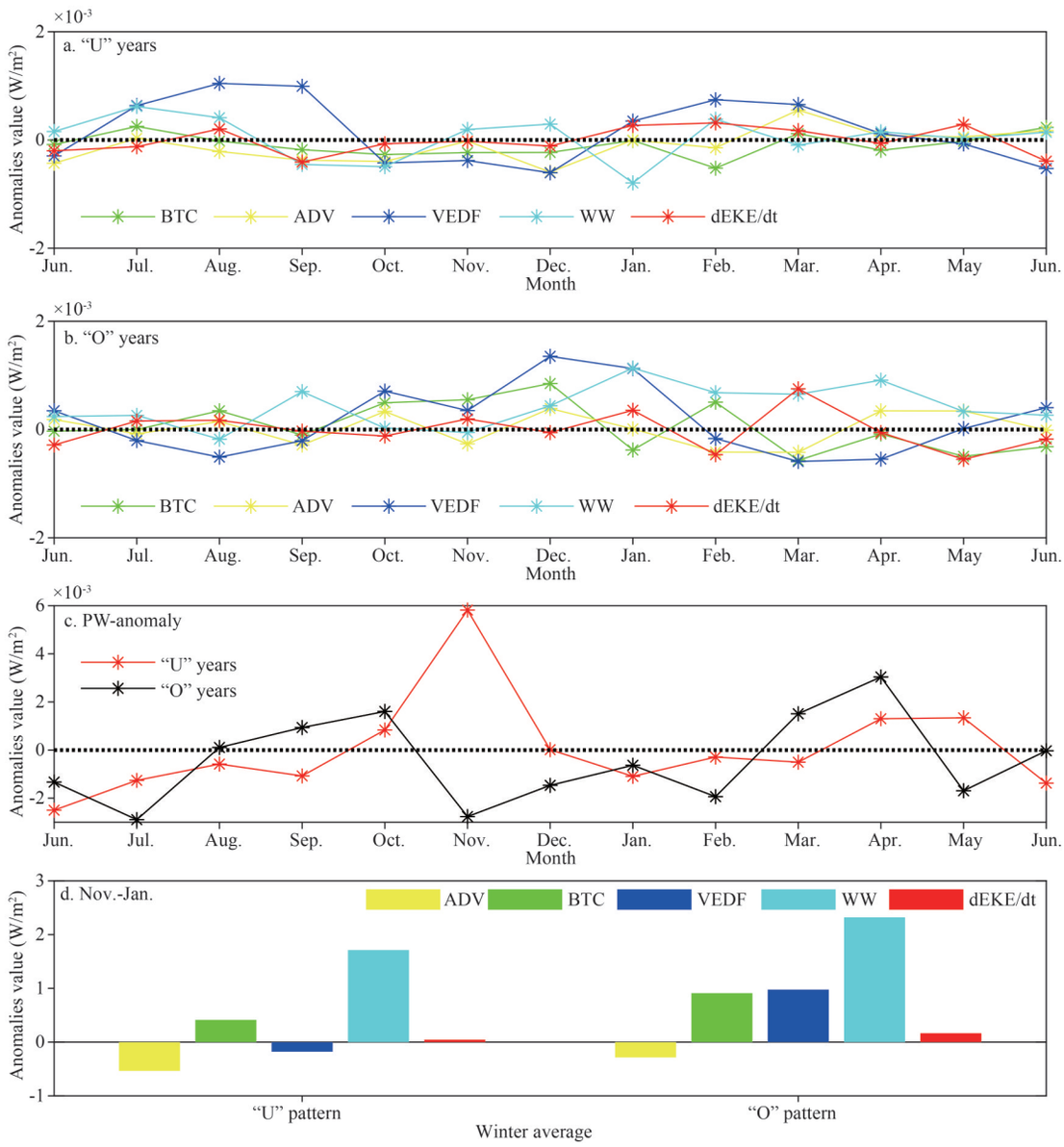

Fig.12 The composite time series of box-average anomalies of BTC, ADV, VEDF, WW, and EKE changes in "U" pattern years (a) and "O" pattern years; PW (c); comparison of box-average anomalies in winter averaged from November to January (d) (unit: W/m²)

The calculation formula of anomalies are as same as Fig.7d.

EKE through the barotropic instability process, while more BTC conversion occurs (Fig.12d, averaged from November to January) during "O" pattern years. Caused by advection, the divergence and convergence of EKE exist along the two sides of SCSwbc (Fig.10a & g). Box-average advection effects corresponds well with EKE changes (Fig.12a–b, yellow lines), implying that ADV may be more important for regulating the interannual change of EKE, while the box-average ADV is smaller than other terms. Terms of WW, BTC, and VEDF are all important to the change of EKE for "U"/"O" two-type winter circulation respectively. In winter with "O" type, the WW, BTC both strengthen, and potential energy is released to kinetic energy, thus EKE increases.

Due to the lack of DIFF term, it is challenging to balance the EKE, which indicates that the energy conversion process between eddies and the surrounding area perhaps could be affected by some other factors. Since the EKE energy balance budget formula depends on the conservation of the region, the selected study area in the western SCS is difficult to meet the conservation conditions of accurate closure, coupled with the neglect of the friction dissipation term, the OFES model bias itself, the error caused by the selection of integral depth, and other factors et al. Thus, above mentions problems both result in large errors of calculations. Nevertheless, quantitative analysis of the EKE balance equation can provide insights for understanding the source and sink of EKE energy, the change of EKE over time, and its influencing factors.

In the following part, the difference in each term averaged in the study area in the two patterns is discussed from a quantitative point of view, as shown in Fig.13. The largest source of EKE energy is the wind stress, which transmits energy to EKE continuously and steadily. However, WW remains at a high level in both patterns, indicating that WW is not the main direct factor to affect the interannual variability of EKE in two-type SCSwbc. In addition to WW, BTC is another energy source of EKE that is significantly different in the two patterns, indicating that the energy converted from MKE to EKE is significantly affected by different types of SCSwbc. In pattern "O", the weakened SCSwbc extends eastward, which considerably enhances BTC, by strengthening the horizontal shear between the eastward deflection branch and surrounding area. In addition, in pattern "O", changes in the density during the east-deflecting process make the VEDF term to be the second largest source of EKE, indicating that a large amount of EPE is converted to EKE through the baroclinic instability process. However, BTC is significantly weakened and VEDF is negative, implying that the huge difference in BTC and VEDF between the two patterns may be an important factor affecting the interannual variability of EKE in December. PW acts as the main sink of the

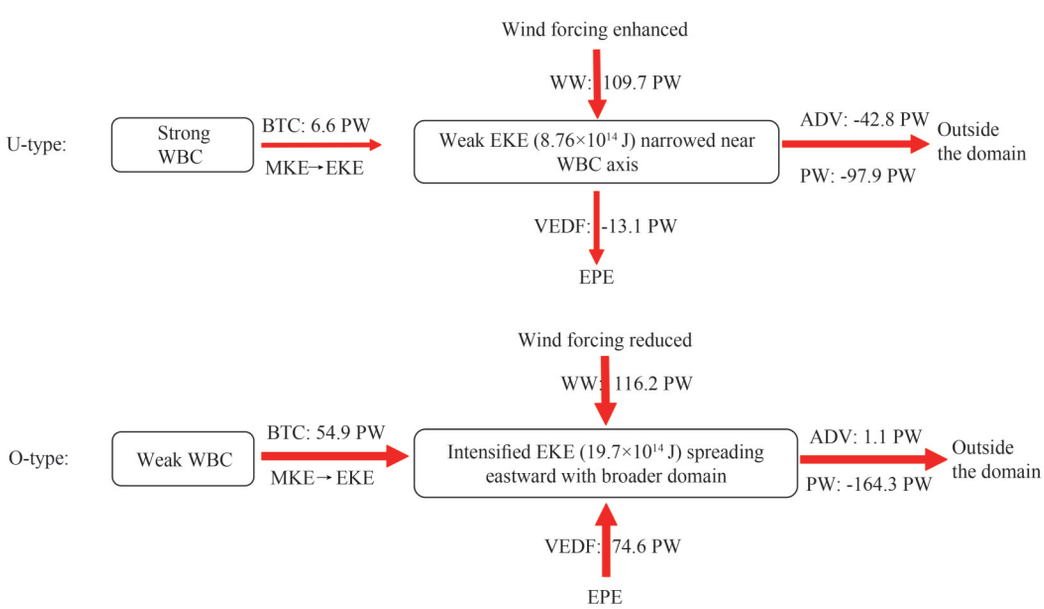

Fig.13 Schematics of EKE budget in the two patterns

The unit of EKE: 10^{14} J; the unit of energy conversions: PW (1 PW=10^7 W).

eddy energy with high values in pattern “O”. The eddy quickly loses a part of its energy to the internal area through pressure differences. ADV is mainly negative in pattern “U”, indicating that the enhanced advection in “U” years causes the loss of EKE to some extent, while vice versa in pattern “O”.

In conclusion, BTC, WW, and VEDF are the main sources of EKE energy. WW is a stable source of EKE energy input, with no significant interannual variation, whereas BTC and VEDF have obvious interannual variation and both increase in pattern “O”, which may be an important reason for strong EKE occurred in pattern “O”. For “U” years, under a strong winter monsoon forcing, the SCSwbc become strong, the WW and BTC from the MKE to EKE are both weak, thus the EKE is weak corresponding to the baroclinic conversion from the kinetic energy to potential energy. The ocean advection draw energy from study domain to outside domain in “U” years. While the situation is reversed in “O” years, and baroclinic conversion transfer the potential energy to kinetic energy. Besides, we can see that the PW is an important factor to cause the EKE energy loss throughout the process, and it reaches a negative peak in “O” years and cancels out the accumulation of EKE by other processes, that is, PW always depresses the kinetic energy in the study domain.

5 DISCUSSION AND SUMMARY

The interannual variability of EKE in the SCS related to two-type western boundary currents in December is investigated based on OFES model outputs from 1993 to 2017. The PC of EOF analysis of KE is used to divide the years into patterns “U”/strong SCSwbc and “O”/weak SCSwbc respectively. The results suggest that in pattern “U”, EKE decreases significantly with the high energy concentrated in a narrow strip along the southeast coast of Vietnam; whereas in pattern “O”, EKE is enhanced significantly and distributes widely by extending eastward to the interior SCS. The correlation between EKE and Niño3.4 indicates that ENSO events affect the interannual variation of EKE in winter to a certain extent. Moreover, during the mature stage of El Niño events, SCSwbc decreases and EKE increases, while the impact of La Niña events is much weaker than that of the El Niño events. By analyzing the relationship among EKE, WSCA, and TSA, we found that the local wind stress forces affected by ENSO events modulate the interannual variation of EKE through the direct and indirect processes. Under the influence of El Niño events, the wind stress forcing weakened SCSwbc and enhanced EKE in pattern “O”, while it is reversed in pattern “U”.

Further, the energy budget is investigated to explore the main factors affecting the interannual variation of EKE in winter, associated with two-type SCSwbc. Results confirm that the wind stress and barotropic/baroclinic instability considerably regulate the EKE in “U” and “O” years. For “U” years, the SCSwbc strengthen, the directly wind work and barotropic conversion from the MKE to EKE are both weak, thus the EKE decreases corresponding to the baroclinic conversion from the kinetic energy to potential energy. At the same time, the ocean advection draw energy from study domain to outside domain. While the situation is reversed in “O” years. For “O” years, the SCSwbc become weak, the directly wind work and barotropic conversion from the MKE to EKE strengthen, thus the EKE increases corresponding to the baroclinic conversion from the potential energy to kinetic energy.

Although wind stress influence is the main energy source of EKE, it is not the major factor regulating the interannual variation of EKE. Further analysis show that the weakening/strengthening of the SCSwbc is mostly corresponding to the weak/strong Kuroshio intrusion. EKE exchanges power with the external ocean environment through the advection term and pressure work. The advection term and pressure work are essential for the power exchange between EKE and the external ocean environment, and they also depend on the selected region. In winter, these two terms greatly reduce the positive work performed by other terms, which indicates that a part of EKE transforms to the outside domain. Overall, ocean energy conversion involves various complex processes, and its accurate characterization is challenging. Therefore, more data and higher-resolution simulations are required to facilitate better understanding of the process.

6 DATA AVAILBILITY STATEMENT

The providers of the data, including the AVISO data (cds.climate.copernicus.eu) and the OFES data (http://apdrc.soest.hawaii.edu/las_ofes/v6/dataset?catitem=2), are greatly appreciated.

7 ACKNOWLEDGMENT

Comments from two anonymous reviewers are

greatly appreciated. The authors also appreciated the contributions of High Performance Computing Division and HPC managers Zhou WEI and Dandan SUI of the South China Sea Institute of Oceanology, Chinese Academy of Sciences.

References

Cai Z Y, Gan J P. 2021. Dynamics of the layered circulation inferred from kinetic energy pathway in the South China Sea. *Journal of Physical Oceanography*, **51**(5): 1671-1685, https://doi.org/10.1175/JPO-D-20-0226.1.

Chelton D B, Schlax M G, Samelson R M et al. 2011. Global observations of nonlinear mesoscale eddies. *Progress in Oceanography*, **91**(2): 167-216, https://doi.org/10.1016/j.pocean.2011.01.002.

Chen C L, Wang G H. 2014. Interannual variability of the eastward current in the western South China Sea associated with the summer Asian monsoon. *Journal of Geophysical Research*: *Oceans*, **119**(9): 5745-5754, https://doi.org/10.1002/2014JC010309.

Chen G X, Hou Y J, Chu X Q et al. 2009. The variability of eddy kinetic energy in the South China Sea deduced from satellite altimeter data. *Chinese Journal of Oceanology and Limnology*, **27**(4): 943-954, https://doi.org/10.1007/s00343-009-9297-6.

Chen G X, Hou Y J, Chu X Q. 2011. Mesoscale eddies in the South China Sea: mean properties, spatiotemporal variability, and impact on thermohaline structure. *Journal of Geophysical Research*: *Oceans*, **116**(C6): C06018, https://doi.org/10.1029/2010jc006716.

Chen G X, Hou Y J, Zhang Q L et al. 2010. The eddy pair off eastern Vietnam: interannual variability and impact on thermohaline structure. *Continental Shelf Research*, **30**(7): 715-723, https://doi.org/10.1016/j.csr.2009.11.013.

Chen G X, Wang D X, Dong C M et al. 2015. Observed deep energetic eddies by seamount wake. *Scientific Reports*, **5**(1): 17416, https://doi.org/10.1038/srep17416.

Chen G X, Xue H J. 2014. Westward intensification in marginal seas. *Ocean Dynamics*, **64**(3): 337-345, https://doi.org/10.1007/s10236-014-0691-z.

Cheng X H, Qi Y Q. 2010. Variations of eddy kinetic energy in the South China Sea. *Journal of Oceanography*, **66**(1): 85-94, https://doi.org/10.1007/s10872-010-0007-y.

Chu X Q, Chen G X, Qi Y Q. 2020. Periodic mesoscale eddies in the South China Sea. *Journal of Geophysical Research*: *Oceans*, **125**(1): e2019JC015139, https://doi.org/10.1029/2019JC015139.

Chu X Q, Dong C M, Qi Y Q. 2017. The influence of ENSO on an oceanic eddy pair in the South China Sea. *Journal of Geophysical Research*: *Oceans*, **122**(3): 1643-1652, https://doi.org/10.1002/2016jc012642.

Chu X Q, Xue H J, Qi Y Q et al. 2014. An exceptional anticyclonic eddy in the South China Sea in 2010. *Journal of Geophysical Research*: *Oceans*, **119**(2): 881-897, https://doi.org/10.1002/2013JC009314.

Dale W. 1956. Wind and drift current in the South China Sea. *The Malayan Journal of Tropical Geography*, **8**: 1-31.

Dong C M, McWilliams J C, Liu Y et al. 2014. Global heat and salt transports by eddy movement. *Nature Communications*, **5**(1): 3294, https://doi.org/10.1038/ncomms4294.

Ducet N, Le Traon P Y. 2001. A comparison of surface eddy kinetic energy and Reynolds stresses in the Gulf Stream and the Kuroshio Current systems from merged TOPEX/Poseidon and ERS-1/2 altimetric data. *Journal of Geophysical Research*: *Oceans*, **106**(C8): 16603-16622, https://doi.org/10.1029/2000JC000205.

Fang G H, Wang G, Fang Y et al. 2012. A review on the South China Sea western boundary current. *Acta Oceanologica Sinica*, **31**(5): 1-10, https://doi.org/10.1007/s13131-012-0231-y.

Fang W D, Fang G H, Shi P et al. 2002. Seasonal structures of upper layer circulation in the southern South China Sea from in situ observations. *Journal of Geophysical Research*: *Oceans*, **107**(C11): 3202, https://doi.org/10.1029/2002JC001343.

Feng B X, Liu H L, Lin P F et al. 2017. Meso-scale eddy in the South China Sea simulated by an eddy-resolving ocean model. *Acta Oceanologica Sinica*, **36**(5): 9-25, https://doi.org/10.1007/s13131-017-1058-3.

Feng B X, Liu H L, Lin P F. 2020. Effects of Kuroshio intrusion optimization on the simulation of mesoscale eddies in the northern South China Sea. *Acta Oceanologica Sinica*, **39**(3): 12-24, https://doi.org/10.1007/s13131-020-1565-5.

Feng M, Wijffels S, Godfrey S et al. 2005. Do eddies play a role in the momentum balance of the Leeuwin Current? *Journal of Physical Oceanography*, **35**(6): 964-975, https://doi.org/10.1175/JPO2730.1.

Frenger I, Gruber N, Knutti R et al. 2013. Imprint of Southern Ocean eddies on winds, clouds and rainfall. *Nature Geoscience*, **6**(8): 608-612, https://doi.org/10.1038/ngeo1863.

Gan J P, Li H, Curchitser E N et al. 2006. Modeling South China Sea circulation: response to seasonal forcing regimes. *Journal of Geophysical Research*: *Oceans*, **111**(C6): C06034, https://doi.org/10.1029/2005JC003298.

Gan J P, Qu T D. 2008. Coastal jet separation and associated flow variability in the southwest South China Sea. *Deep Sea Research Part I*: *Oceanographic Research Papers*, **55**(1): 1-19, https://doi.org/10.1016/j.dsr.2007.09.008.

Geng W, Xie Q, Chen G X et al. 2016. Numerical study on the eddy-mean flow interaction between a cyclonic eddy and Kuroshio. *Journal of Oceanography*, **72**(5): 727-745, https://doi.org/10.1007/s10872-016-0366-0.

Guo Z X, Yang T H, Qiu D Z. 1985. The South China Sea Warm current and the SW-ward current on its right side in winter. *Tropic Oceanology*, **4**(1): 1-9. (in Chinese with English abstract)

He Q Y, Zhan H G, Cai S Q et al. 2018. A new assessment of mesoscale eddies in the South China Sea: surface features, three-dimensional structures, and thermohaline transports. *Journal of Geophysical Research*: *Oceans*, **123**(7): 4906-4929, https://doi.org/10.1029/2018JC014054.

He Q Y, Zhan H G, Xu J et al. 2019. Eddy-induced

chlorophyll anomalies in the western South China Sea. *Journal of Geophysical Research*: *Oceans*, **124**(12): 9487-9506, https://doi.org/10.1029/2019JC015371.

He Z G, Wang D X. 2009. Surface pattern of the South China Sea western boundary current in winter. *In*: Gan, J ed. Advances in Geosciences. World Scientific Publishing Co Pte Ltd., 128 Farred RD, Singapore. Volume 12: Ocean Science. p. 99-107, https://doi.org/10.1142/9789812836168_0008.

Ho C R, Kuo N J, Zheng Q A et al. 2000. Dynamically active areas in the South China Sea detected from TOPEX/Poseidon satellite altimeter data. *Remote Sensing of Environment*, **71**(3): 320-328, https://doi.org/10.1016/S0034-4257(99)00094-2.

Holloway G. 1986. Estimation of oceanic eddy transports from satellite altimetry. *Nature*, **323**(6085): 243-244, https://doi.org/10.1038/323243a0.

Hu J Y, Kawamura H, Hong H S et al. 2000. A review on the currents in the South China Sea: seasonal circulation, South China Sea Warm current and Kuroshio Intrusion. *Journal of Oceanography*, **56**(6): 607-624, https://doi.org/10.1023/A:1011117531252.

Hu J Y, Zheng Q A, Sun Z Y et al. 2012. Penetration of nonlinear Rossby eddies into South China Sea evidenced by cruise data. *Journal of Geophysical Research*: *Oceans*, **117**(C3): C03010, https://doi.org/10.1029/2011jc007525.

Hu S J, Sprintall J, Guan C et al. 2020. Deep-reaching acceleration of global mean ocean circulation over the past two decades. *Science Advances*, **6**(6): eaax7727, https://doi.org/10.1126/sciadv.aax7727.

Hurlburt H E, Metzger E J, Hogan P J et al. 2008. Steering of upper ocean currents and fronts by the topographically constrained abyssal circulation. *Dynamics of Atmospheres and Oceans*, **45**(3-4): 102-134, https://doi.org/10.1016/j.dynatmoce.2008.06.003.

Hwang C, Chen S A. 2000. Circulations and eddies over the South China Sea derived from TOPEX/Poseidon altimetry. *Journal of Geophysical Research*: *Oceans*, **105**(C10): 23943-23965, https://doi.org/10.1029/2000JC900092.

Ivchenko V O, Treguier A M, Best S E. 1997. A kinetic energy budget and internal instabilities in the Fine Resolution Antarctic Model. *Journal of Physical Oceanography*, **27**(1): 5-22, https://doi.org/10.1175/1520-0485(1997)027<0005:AKEBAI>2.0.CO;2.

Kang D J, Curchitser E N. 2015. Energetics of Eddy-mean flow interactions in the gulf stream region. *Journal of Physical Oceanography*, **45**(4): 1103-1120, https://doi.org/10.1175/JPO-D-14-0200.1.

Kubryakov A A, Kozlov I E, Manucharyan G E. 2021. Large mesoscale eddies in the Western Arctic Ocean from satellite altimetry measurements. *Journal of Geophysical Research*: *Oceans*, **126**(5): e2020JC016670, https://doi.org/10.1029/2020JC016670.

Li H, Wang Q, Huang K et al. 2017. Characteristics of eddy-mean flow interaction in the offshore current area of western South China Sea. *Oceanologia et Limnologia Sinica*, **48**(5): 912-925, http://doi.org/10.11693/hyhz20170400086. (in Chinese with English abstract)

Li Y L, Han W Q, Wilkin J L et al. 2014. Interannual variability of the surface summertime eastward jet in the South China Sea. *Journal of Geophysical Research*: *Oceans*, **119**(10): 7205-7228, https://doi.org/10.1002/2014JC010206.

Lin P F, Wang F, Chen Y L et al. 2007. Temporal and spatial variation characteristics on eddies in the South China Sea I. Statistical analyses. *Acta Oceanologica Sinica*, **29**(3): 14-22, https://doi.org/10.3321/j.issn:0253-4193.2007.03.002. (in Chinese with English abstract)

Liu Q Y, Feng M, Wang D X. 2011. ENSO-induced interannual variability in the southeastern South China Sea. *Journal of Oceanography*, **67**(1): 127-133, https://doi.org/10.1007/s10872-011-0002-y.

Liu Q Y, Huang R X, Wang D X. 2012. Implication of the South China Sea throughflow for the interannual variability of the regional upper-ocean heat content. *Advances in Atmospheric Sciences*, **29**(1): 54-62, https://doi.org/10.1007/s00376-011-0068-x.

Liu Q Y, Jia Y L, Liu P H et al. 2001. Seasonal and intraseasonal thermocline variability in the central South China Sea. *Geophysical Research Letters*, **28**(23): 4467-4470, https://doi.org/10.1029/2001GL013185.

Lyu K W, Yang X Y, Zheng Q A et al. 2016. Intraseasonal variability of the winter western boundary current in the South China Sea using satellite data and mooring observations. *IEEE Journal of Selected Topics in Applied Earth Observations and Remote Sensing*, **9**(11): 5079-5088, https://doi.org/10.1109/JSTARS.2016.2553049.

Ma X H, Jing Z, Chang P et al. 2016. Western boundary currents regulated by interaction between ocean eddies and the atmosphere. *Nature*, **535**(7613): 533-537, https://doi.org/10.1038/nature18640.

McGillicuddy D J Jr, Anderson L A, Bates N R et al. 2007. Eddy/wind interactions stimulate extraordinary mid-ocean plankton blooms. *Science*, **316**(5827): 1021-1026, https://doi.org/10.1126/science.1136256.

Metzger E J, Hurlburt H E. 2001. The nondeterministic nature of Kuroshio penetration and eddy shedding in the South China Sea. *Journal of Physical Oceanography*, **31**(7): 1712-1732, https://doi.org/10.1175/1520-0485(2001)031<1712:Tnnokp>2.0.Co;2.

Ni Q B, Zhai X M, Wang G H et al. 2020. Widespread mesoscale dipoles in the global ocean. *Journal of Geophysical Research*: *Oceans*, **125**(10): e2020JC016479, https://doi.org/10.1029/2020JC016479.

Qiu B, Chen S M, Schneider N, 2014. A coupled decadal prediction of the dynamic state of the Kuroshio extension system. *Journal of Climate*, **27**(4): 1751-1764, https://doi.org/10.1175/JCLI-D-13-00318.1.

Qu T D, Du Y, Sasaki H. 2006. South China Sea throughflow: a heat and freshwater conveyor. *Geophysical Research Letters*, **33**(23): L23617, https://doi.org/10.1029/2006GL028350.

Quan Q, Xue H J, Qin H L et al. 2016. Features and variability of the South China Sea western boundary current from 1992 to 2011. *Ocean Dynamics*, **66**(6): 795-810, https://doi.org/10.1007/s10236-016-0951-1.

Sasaki H, Nonaka M, Masumoto Y et al. 2008. An eddy-resolving hindcast simulation of the quasiglobal ocean from 1950 to 2003 on the Earth Simulator. *In*: Hamilton K, Ohfuchi W eds. High Resolution Numerical Modelling of the Atmosphere and Ocean. Springer, New York. p.157-185, https://doi.org/10.1007/978-0-387-49791-4_10.

Sasaki H, Sasai Y, Kawahara S et al. 2004. A series of eddy-resolving ocean simulations in the world ocean-OFES (OGCM for the Earth Simulator) project. *In*: Oceans' 04 MTS/IEEE Techno-Ocean'04 (IEEECat. No. 04CH3760 0). IEEE, Kobe. p.1535-1541, https://doi.org/10.1109/OCEANS.2004.1406350.

Shaw P T, Chao S Y, Fu L L. 1999. Sea surface height variations in the South China Sea from satellite altimetry. *Oceanologica Acta*, **22**(1): 1-17, https://doi.org/10.1016/S0399-1784(99)80028-0.

Shu Y Q, Xue H J, Wang D X et al. 2016. Observed evidence of the anomalous South China Sea western boundary current during the summers of 2010 and 2011. *Journal of Geophysical Research*: *Oceans*, **121**(2): 1145-1159, https://doi.org/10.1002/2015JC011434.

Su J Z, Lu J, Hou Y J et al. 2002. Analysis of satellite-tracked drifting buoys in the South China Sea. *Oceanologia et Limnologia Sinica*, **33**(2): 121-127, https://doi.org/10.3321/j.issn:0029-814X.2002.02.002. (in Chinese with English abstract)

Su J L, Xu J P, Cai S Q et al. 1999. Gyres and eddies in the South China Sea. *In*: Ding Y H, Li C Y eds. Onset and Evolution of the South China Sea Monsoon and its Interaction with the Ocean. Beijing Meteorological Press, Beijing, China. p.272-279.

Sun W J, Dong C M, Wang R Y et al. 2017. Vertical structure anomalies of oceanic eddies in the Kuroshio Extension region. *Journal of Geophysical Research*: *Oceans*, **122**(2): 1476-1496, https://doi.org/10.1002/2016JC01222.

Sun Y, Lan J. 2021. Summertime eastward jet and its relationship with western boundary current in the South China Sea on the interannual scale. *Climate Dynamics*, **56**(3): 935-947, https://doi.org/10.1007/s00382-020-05511-z.

Sun Z B, Zhang Z W, Zhao W et al. 2016. Interannual modulation of eddy kinetic energy in the northeastern South China Sea as revealed by an eddy-resolving OGCM. *Journal of Geophysical Research*: *Oceans*, **121**(5): 3190-3201, https://doi.org/10.1002/2015JC011497.

Tuo P F, Yu J Y, Hu J Y. 2019. The changing influences of ENSO and the Pacific meridional mode on mesoscale eddies in the South China Sea. *Journal of Climate*, **32**(3): 685-700, https://doi.org/10.1175/JCLI-D-18-0187.1.

Wang C Z, Wang W Q, Wang D X et al. 2006a. Interannual variability of the South China Sea associated with El Niño. *Journal of Geophysical Research*: *Ocean*, **111**(C3): C03023, https://doi.org/10.1029/2005JC003333.

Wang D X, Liu Q Y, Huang R X et al. 2006b. Interannual variability of the South China Sea throughflow inferred from wind data and an ocean data assimilation product. *Geophysical Research Letters*, **33**(14): L14605, https://doi.org/10.1029/2006GL026316.

Wang D X, Liu Q Y, Xie Q et al. 2013a. Progress of regional oceanography study associated with western boundary current in the South China Sea. *Chinese Science Bulletin*, **58**(11): 1205-1215, https://doi.org/10.1007/s11434-012-5663-4.

Wang D X, Wang Q, Zhou W D et al. 2013b. An analysis of the current deflection around Dongsha Islands in the northern South China Sea. *Journal of Geophysical Research*: *Oceans*, **118**(1): 490-501, https://doi.org/10.1029/2012JC008429.

Wang D X, Xiao J G, Shu Y Q et al. 2016. Progress on deep circulation and meridional overturning circulation in the South China Sea. *Science China Earth Sciences*, **59**(9): 1827-1833, https://doi.org/10.1007/s11430-016-5324-6.

Wang D X, Xu H Z, Lin J et al. 2008a. Anticyclonic eddies in the northeastern South China Sea during winter 2003/2004. *Journal of Oceanography*, **64**(6): 925-935, https://doi.org/10.1007/s10872-008-0076-3.

Wang G H, Chen D K, Su J L. 2008b. Winter eddy genesis in the eastern South China Sea due to orographic wind jets. *Journal of Physical Oceanography*, **38**(3): 726-732, https://doi.org/10.1175/2007jpo3868.1.

Wang G H, Su J L, Chu P C. 2003. Mesoscale eddies in the South China Sea observed with altimeter data. *Geophysical Research Letters*, **30**(21): 2121, https://doi.org/10.1029/2003GL018532.

Wang L P, Koblinsky C J, Howden S. 2000. Mesoscale variability in the South China Sea from the TOPEX/Poseidon altimetry data. *Deep Sea Research Part I*: *Oceanographic Research Papers*, **47**(4): 681-708, https://doi.org/10.1016/S0967-0637(99)00068-0.

Wang Q, Zeng L L, Shu Y Q et al. 2019. Energetic topographic Rossby waves in the northern South China Sea. *Journal of Physical Oceanography*, **49**(10): 2697-2714, https://doi.org/10.1175/JPO-D-18-0247.1.

Wang Q, Zeng L L, Shu Y Q et al. 2020. Interannual variability of South China Sea winter circulation: response to Luzon Strait transport and El Niño wind. *Climate Dynamics*, **54**(1-2): 1145-1159, https://doi.org/10.1007/s00382-019-05050-2.

Wyrtki K. 1961. Physical Oceanography of the Southeast Asian Waters. Scripps Institution of Oceanography, University of California, La Jolla. p.1-195.

Xie S P, Xie Q, Wang D X et al. 2003. Summer upwelling in the South China Sea and its role in regional climate variations. *Journal of Geophysical Research*: *Oceans*, **108**(C8): 3261, https://doi.org/10.1029/2003JC001867.

Xiu P, Chai F, Shi L et al. 2010. A census of eddy activities in the South China Sea during 1993-2007. *Journal of Geophysical Research*: *Oceans*, **115**(C3): C03012, https://doi.org/10.1029/2009JC005657.

Xue H J, Chai F, Pettigrew N et al. 2004. Kuroshio intrusion and the circulation in the South China Sea. *Journal of Geophysical Research*: *Oceans*, **109**(C2): C02017, https://doi.org/10.1029/2002JC001724.

Yang H Y, Wu L X, Liu H L et al. 2013. Eddy energy sources and sinks in the South China Sea. *Journal of Geophysical Research*: *Oceans*, **118**(9): 4716-4726, https://doi.org/10.

1002/jgrc.20343.

Yao J L, Li H, Liu Q Y et al. 2017. Energy diagnostic of the mesoscale processes loaded by the South China Sea throughflow. *Oceanologia et Limnologia Sinica*, **48**(6): 1257-1268, http://doi.org/10.11693/hyhz20170800207. (in Chinese with English abstract)

Yuan D L, Han W Q, Hu D X. 2007. Anti-cyclonic eddies northwest of Luzon in summer-fall observed by satellite altimeters. *Geophysical Research Letters*, **34**(13): L13610, https://doi.org/10.1029/2007GL029401.

Zhang N N, Liu G Q, Liu Q Y et al. 2020. Spatiotemporal Variations of Mesoscale Eddies in the Southeast Indian Ocean. *Journal of Geophysical Research*: *Oceans*, **125**(8): e2019JC015712, https://doi.org/10.1029/2019JC015712.

Zheng S J, Feng M, Du Y et al. 2018. Interannual variability of eddy kinetic energy in the subtropical southeast Indian Ocean associated with the El Niño-Southern Oscillation. *Journal of Geophysical Research*: *Oceans*, **123**(2): 1048-1061, https://doi.org/10.1002/2017JC013562.

Zhou H, Yuan D L, Li R X et al. 2010. The western South China Sea currents from measurements by Argo profiling floats during October to December 2007. *Chinese Journal of Oceanology and Limnology*, **28**(2): 398-406, https://doi.org/10.1007/s00343-010-9052-z.

Zhu X H, Zhao R X, Guo X Y et al. 2015. A long-term volume transport time series estimated by combining in situ observation and satellite altimeter data in the northern South China Sea. *Journal of Oceanography*, **71**(6): 663-673, https://doi.org/10.1007/s10872-015-0305-5.

Zhuang W, Xie S P, Wang D X et al. 2010. Intraseasonal variability in sea surface height over the South China Sea. *Journal of Geophysical Research*: *Oceans*, **115**(C4): C04010, https://doi.org/10.1029/2009JC005647.

Zu T T, Wang D X, Wang Q et al. 2020. A revisit of the interannual variation of the South China Sea upper layer circulation in summer: correlation between the eastward jet and northward branch. *Climate Dynamics*, **54**(1-2): 457-471, https://doi.org/10.1007/s00382-019-05007-5.

Zu T T, Xue H J, Wang D X et al. 2019. Interannual variation of the South China Sea circulation during winter: intensified in the southern basin. *Climate Dynamics*, **52**(3-4): 1917-1933, https://doi.org/10.1007/s00382-018-4230-3.